Effect of sulfuric acid coating on heterogeneous ice nucleation by soot aerosol particles

O. Möhler,[1] S. Büttner,[1] C. Linke,[1] M. Schnaiter,[1] H. Saathoff,[1] O. Stetzer,[1] R. Wagner,[1] M. Krämer,[2] A. Mangold,[2] V. Ebert,[3] and U. Schurath[1]

Received 28 June 2004; revised 26 November 2004; accepted 23 March 2005; published 14 June 2005.

[1] The low-temperature aerosol and cloud chamber AIDA (Aerosol Interactions and Dynamics in the Atmosphere) of Forschungszentrum Karlsruhe was used to investigate the effect of sulfuric acid coating on the ice nucleation efficiency of soot aerosol particles from a spark discharge generator. The uncoated (sulfuric acid–coated) soot aerosol showed a nearly lognormal size distribution with number concentrations of 300–5000 cm^{-3} (2500–56,000 cm^{-3}), count median diameters of 70–140 nm (90–200 nm), and geometric standard deviation of 1.3–1.4 (1.5–1.6). The volume fraction of the sulfuric acid coating to the total aerosol volume concentration ranged from 21 to 81%. Ice activation was investigated in dynamic expansion experiments simulating cloud cooling rates between about −0.6 and −3.5 K min^{-1}. At temperatures between 186 and ~235 K, uncoated soot particles acted as deposition nuclei at very low ice saturation ratios between 1.1 and 1.3. Above 235 K, ice nucleation only occurred after approaching liquid saturation. Coating with sulfuric acid significantly increased the ice nucleation thresholds of soot aerosol to saturation ratios increasing from ~1.3 at 230 K to ~1.5 at 185 K. This immersion mode of freezing nucleates ice well below the thresholds for homogeneous freezing of pure sulfuric acid solution droplets measured in previous AIDA experiments. A case study indicated that in contrast to the homogeneous freezing the nucleation rate of the immersion freezing mechanism depends only weakly on relative humidity and thereby the solute concentration. These results show that it is important to know the mixing state of soot and sulfuric acid aerosol particles in order to properly assess their role in cirrus formation.

Citation: Möhler, O., et al. (2005), Effect of sulfuric acid coating on heterogeneous ice nucleation by soot aerosol particles, *J. Geophys. Res.*, *110*, D11210, doi:10.1029/2004JD005169.

1. Introduction

[2] Homogeneous freezing of supercooled solution droplets, mainly consisting of sulfuric acid, has been emphasized in numerous studies to play an important role for the formation and radiative properties of cirrus [*Sassen and Dodd*, 1988; *Sassen et al.*, 1989; *Heymsfield and Sabin*, 1989; *Jensen and Toon*, 1992; *Haag et al.*, 2003b; *Kärcher and Ström*, 2003] and wave clouds [*Heymsfield and Miloshevich*, 1993; *Jensen et al.*, 1998; *Field et al.*, 2001]. New parameterizations have been developed [*Kärcher and Lohmann*, 2002a, 2002b] and applied in a climate model [*Lohmann and Kärcher*, 2002] for calculating the ice crystal number concentration in upper tropospheric clouds as a function of the ambient temperature, the updraft velocity, and aerosol parameters. The ice crystal number concentration is a key parameter for estimating the mean crystal size and therefore the radiative properties of cirrus clouds in numerical models.

[3] On the other hand, cirrus formation may also be influenced by heterogeneous ice nucleation on the surface of solid aerosol particles. Specific surface properties can markedly lower the ice supersaturation threshold compared to homogeneous freezing [*Pruppacher and Klett*, 1997], thereby eventually changing not only the occurrence frequency but also the microphysical and optical properties of cirrus clouds. Chemical analysis of single aerosol particles revealed sulfur, carbonaceous, mineral, and metallic compounds as major fractions of the upper tropospheric and lower-stratospheric aerosol [*Twohy and Gandrud*, 1998; *Chen et al.*, 1998; *Cziczo et al.*, 2004]. Chemical analysis of ice nuclei and ice particle residuals in the upper troposphere by the same authors showed similar results, analysis of ice particles and residual particles from aircraft contrails showed a somewhat higher fraction of metallic compounds [*Chen et al.*, 1998].

[4] Externally mixed sulfuric acid and soot particles and sulfuric acid–coated soot particles formed in contrail plumes by chemical and microphysical processes may

[1]Institute for Meteorology and Climate Research, Forschungszentrum Karlsruhe, Karlsruhe, Germany.
[2]Institut für Chemie und Dynamik der Geosphäre I, Forschungszentrum Jülich, Jülich, Germany.
[3]Physikalisch-Chemisches Institut, Universität Heidelberg, Heidelberg, Germany.

0148-0227/05/2004JD005169

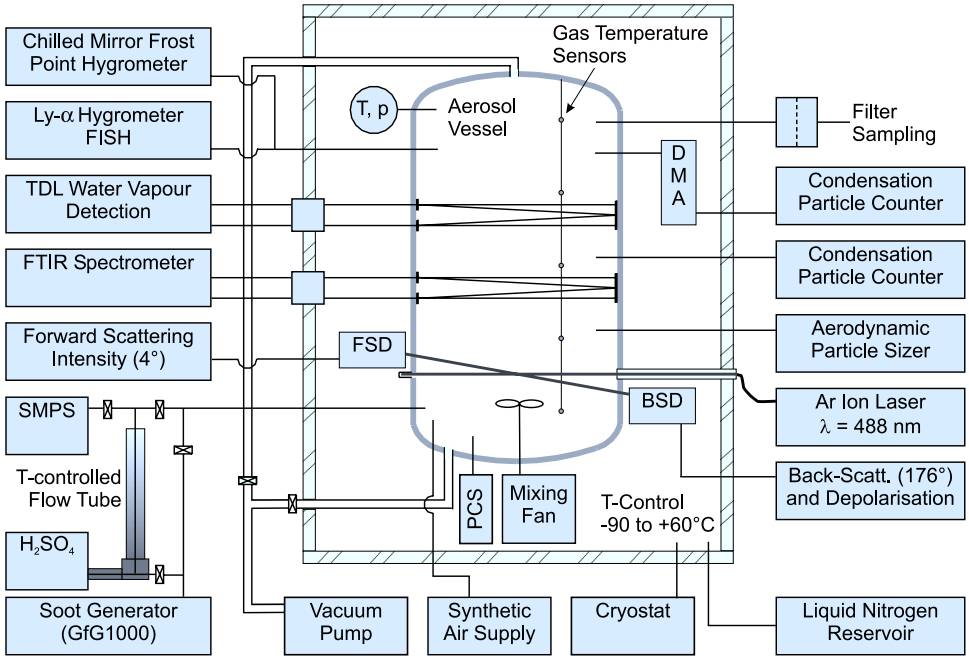

Figure 1. Schematic view of the AIDA experimental facility showing major technical components and scientific instrumentation used for ice activation experiments.

significantly contribute to the upper tropospheric and lower-stratospheric aerosol [*Rahmes et al.*, 1998; *Ferry et al.*, 1999]. The amount of particulate sulfuric acid in aircraft exhaust plumes depends on the fuel sulfur content and the factor of sulfur(IV) to sulfur(VI) conversion [*Miake-Lye et al.*, 1998; *Pueschel et al.*, 1998; *Schumann et al.*, 2002; *Curtius et al.*, 2002]. Sulfuric acid can either contribute to the formation of new particles in the plume by binary nucleation with water molecules or condense on soot particles also emitted by the engine [*Andronache and Chameides*, 1997; *Kärcher*, 1998a]. Direct measurements in aircraft plumes have been made of the mass and number concentrations of volatile (sulfuric acid) and nonvolatile (soot) particles [*Hagen et al.*, 1998; *Anderson et al.*, 1998; *Paladino et al.*, 1998; *Pueschel et al.*, 1998; *Schröder et al.*, 1998]. Despite significant progress concerning the physical and chemical characterization of aircraft emissions there is still lack of quantitative data on, e.g., the sulfuric acid and organic carbon coating of individual particles. Recent investigations also addressed the effect of the organic carbon (OC) content on the hygroscopic properties of soot particles emitted from ground test engines [*Petzold et al.*, 2003]. According to these and also previous studies by *Petzold and Schröder* [1998] soot emitted by aircraft engines may contain up to 30% OC. *Hitzenberger et al.* [2003] argued that the OC content could explain larger apparent diameters for CCN activation at ~0.7% supersaturation compared to a coated sphere model taking pure sulfuric acid as coating material.

[5] Numerous experimental and modeling studies investigated the impact of aircraft-emitted sulfuric acid and soot particles on contrails [*Andronache and Chameides*, 1997; *Kärcher*, 1998b; *Miake-Lye et al.*, 1998], cirrus clouds [*Jensen and Toon*, 1997; *Kärcher*, 1998b; *Kristensson et al.*, 2000], and related radiative transfer issues [*Rahmes et al.*, 1998; *Penner et al.*, 1999]. Nevertheless, the contribution of aircraft particulate emissions and solid aerosol particles from other sources to the global climate and its projection to future climate change is very uncertain [*Penner et al.*, 1999]. One reason for that is lack of knowledge about the relation between atmospheric aerosol particles and the occurrence frequency, persistence, and optical properties of cirrus clouds. Little is known about the impact of aerosol properties on the formation rates of ice crystals by heterogeneous ice nucleation modes. Previous laboratory studies found soot aerosol from an acetylene burner to be active as immersion freezing nuclei at temperatures below about −16°C [*DeMott*, 1990]. The same study also investigated the transition from immersion to homogeneous freezing of water droplets condensed on the soot particles. More recently, *DeMott et al.* [1999] found redispersed soot particles from an industrial source (Degussa lamp black) to nucleate ice at temperatures below 233 K more efficiently if coated with sulfuric acid. In the present paper we investigate, in different series of laboratory simulation experiments of cloud formation processes, the effect of soot particles immersed in sulfuric acid aerosol droplets on ice nucleation thresholds and rates compared to the ice nucleation initiated by pure soot and sulfuric acid particles.

2. Experimental Methods and Parameters

2.1. Cloud Chamber Expansion Method

[6] Ice nucleation experiments were performed at the AIDA aerosol chamber facility of Forschungszentrum Karlsruhe [*Nink et al.*, 2000; *Möhler et al.*, 2001]. The operation of the AIDA facility as a moderate expansion cloud chamber for ice nucleation studies is described in detail by *Möhler et al.* [2003] and will only briefly be reviewed here. Figure 1 schematically shows the AIDA facility with the scientific instrumentation used for the experiments discussed in this paper. Major technical com-

ponents are the large cold box which encloses the cylindrical aerosol vessel, the vacuum system, and the air supply system. The aerosol vessel (4 m diameter, 84 m^3 volume) is made of 2 cm thick aluminum walls. Access to the chamber is given on 39 flanges with various feedthroughs for sensors, tubes for sampling instruments, and windows for optical in situ measurements.

[7] The interior of the thermally insulated cold box can be cooled to any temperature down to 183 K. Air ventilation between the walls of the cold box and the aerosol vessel at an upward directed flow of 28,000 m^3 h^{-1} maintains homogeneous temperature conditions with spatial and temporal fluctuations of less than 0.6 K throughout the entire box. The air is passed through two heat exchangers cooled by evaporation of a cooling liquid (R404A) to 235 K, or by liquid nitrogen evaporation to 183 K.

[8] Two vacuum pumps evacuate the vessel within ~1 hour to a pressure below 1 hPa mainly for removing remnants of previous experiments and providing clean and aerosol free experimental conditions. Further effective cleaning is achieved by flushing and pumping cycles at pressures below 10 hPa where the system reaches its maximum pumping speed of ~1500 m^3 h^{-1}. Particle free synthetic air is used for flushing as well as for filling the evacuated vessel to atmospheric pressure. A pumping, flushing and filling cycle needs ~3 h. The pumping system is also used to achieve ice supersaturated conditions inside the aerosol vessel by controlled pumping as described below.

[9] Before starting ice nucleation experiments, the inner wall of the aerosol vessel is coated with a thin ice layer, e.g., by filling the vessel with humidified air at higher temperatures and slowly cooling it to lower temperatures. The ice layer maintains almost ice saturated conditions at lower temperatures. After uniform temperature (within 0.6 K) and humidity (within 5%) conditions are reached the aerosol to be studied is added to the aerosol vessel (see section 2.3) and the first ice activation experiment is started. Ice supersaturated conditions are achieved by controlled pumping, typically from 1000 to 800 hPa. Time series of the pressure p and the corresponding rate of pressure change dp/dt are shown in Figure 2 (first panel) for a typical experiment with sulfuric acid–coated soot (CS.B5.2) (see section 2.4 for a summary of the experimental parameters). The time axis is plotted in seconds relative to start pumping defined as the reference time t_0 for all expansion experiments discussed in this paper.

[10] After pumping starts, the gas temperature T_g drops because of volume expansion whereas the wall temperature T_w remains almost constant (Figure 2, second panel). A mixing fan maintains homogeneous temperature and humidity conditions within the entire volume except for a few cm thick boundary transition layer to the vessel walls. Temperatures throughout the mixed part of the volume differ from the mean value by less than 0.3 K. The cooling rate dT_g/dt calculated from the measured temperature profile is compared to the adiabatic cooling rate $(dT/dt)_{adia}$ calculated from dp/dt. The actual cooling rate in the AIDA vessel is close to adiabatic only during the first few seconds of pumping. With further pumping, the cooling rate is steadily diminished by the heat flux from the chamber walls which is increasing with increasing difference between T_w and T_g.

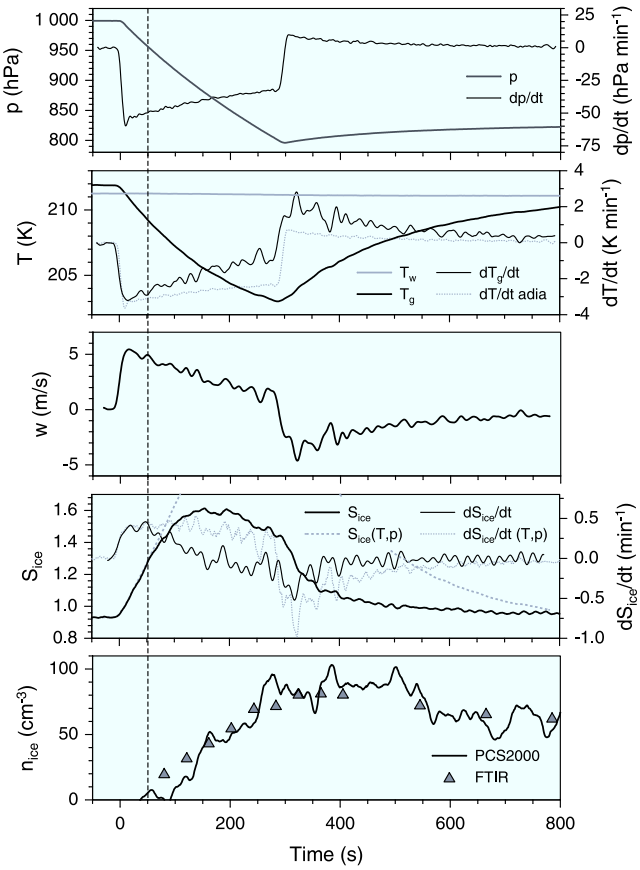

Figure 2. Measured time series of pressure, temperature, ice saturation ratio, and ice particle number concentrations for experiment CS.B5.2 (see Table 2). Calculated rates of temperature, pressure, and saturation ratio change are also shown (see text for more explanations). The vertical wind velocity in the third panel was calculated from the cooling rate shown in the second panel.

[11] To compare with cloud situations, Figure 2 (third panel) shows the equivalent vertical updraft velocity w of an adiabatically expanding air parcel that experiences the same cooling rate as an air parcel in the AIDA chamber. The updraft velocity $w = -(c_p/g) \cdot (dT_g/dt)$ was calculated from the AIDA cooling rate, the specific heat capacity of air c_p = 1005 J K^{-1} kg^{-1} and the acceleration of gravity g = 9.81 m s^{-2}.

[12] Assuming constant water volume mixing ratio, the ice saturation ratio

$$S_{ice}(p,T) = \frac{e_w}{e_{ice}} = \frac{e_w(t_0) \cdot p}{p(t_0) \cdot e_{ice}} \quad (1)$$

is given for both the cloud and the AIDA air parcel as function of T_g and p, with the water vapor pressure e_w and the water vapor saturation pressure with respect to ice

$$\log_{10} e_{ice} = -\frac{2663.5}{T_g} + 12.537 \quad (2)$$

taken from *Marti and Mauersberger* [1993] with T_g in K and e_{ice} in Pa. From this we can calculate the rate of ice saturation increase

$$\frac{dS_{ice}}{dt}(p,T) = -S_{ice}\frac{\Delta H}{RT_g^2}\frac{dT_g}{dt} + \frac{S_{ice}}{p}\frac{dp}{dt} \quad (3)$$

as function of dT_g/dt and dp/dt, with $\Delta H/R$ = ln10 · 2663.5 K. Figure 2 (fourth panel) shows the calculated time profiles of $S_{ice}(p, T)$ (equation (1)) and $dS_{ice}/dt(p, T)$ compared to the respective time profiles calculated from the water vapor pressure e_w directly measured in situ by tunable diode laser (TDL) absorption. The TDL system is based on a room temperature near-infrared tunable diode laser at 1370 ± 2 nm and a 82 m White multipath cell. The data evaluation procedures used are similar to earlier in situ TDL spectrometers, which were developed, e.g., for the simultaneous in situ detection of stratospheric CH_4 and H_2O [*Gurlit et al.*, 2005]. Systematic errors of up to 30%, probably caused by uncertainties of absorption line parameters taken from the literature, have been corrected by comparison with independent measurements of the total water concentration with a chilled mirror and a Lyman-α hygrometer described below. After correction for the systematic errors, the TDL system provided a time resolution of ∼1 Hz, an accuracy of ±5 to ±10%, and a resolution in the water vapor mixing ratio of up to 15 ppb.

[13] Figure 2 (fourth panel) shows S_{ice} and dS_{ice}/dt calculated from the TDL data to agree well with equations (1) and (3) until the onset of ice nucleation indicated by the vertical line. The detection of the onset of ice nucleation will be discussed in the following section. The AIDA expansion experiments therefore simulate both the rates of temperature and ice saturation change of a cloud air parcel rising at a vertical velocity given in Figure 2 (third panel). Different cooling rates can be simulated with different pumping speeds (see section 2.4). After ice particles are formed, dS_{ice}/dt decreases because of water uptake by the growing ice particles, and the ice saturation ratio reaches a peak value determined by the cooling rate, the rate of ice crystal formation, and the ice crystal growth rate (see discussion in section 3.2).

[14] Because T_w remains almost constant during pumping, the water saturation pressure $e_{ice,wall}$ above the ice-coated vessel walls also remains constant whereas the water vapor pressure e_w in the mixed vessel volume linearly decreases with the decreasing pressure during pumping (see equation (1)). The difference $\Delta e_w = e_{ice,wall} - e_w$ causes an increasing flux of water molecules from the ice-coated walls into the aerosol vessel. As shown in Figure 2, this water flux hardly affects the saturation profile until ice particles are formed. The assumption of constant total water mixing ratio is therefore reasonable for investigating ice nucleation onset and dynamics during the AIDA experiments. After ice formation started, the water vapor is steadily depleted by the diffusional flux of water molecules to the increasing ice surface resulting in an increased water flux from the wall which may significantly contribute to the saturation profile and the ice water content. The fluxes and dynamic partitioning of water between the gas phase, the ice particles, and the vessel walls are discussed in more detail by *Mangold et al.* [2005]. The ice particle number densities shown in Figure 2 (fifth panel) will be discussed in sections 2.2 and 3.2.

[15] In addition to the water vapor, the total water concentration $e_{w,t}$ is also measured at a time resolution of ∼1 s with the Lyman-α hygrometer FISH of Forschungszentrum Jülich [*Zöger et al.*, 1999] and, at a somewhat slower response time depending on the actual water mixing ratio, with a fast chilled mirror hygrometer (MBW, Model 373). For $e_{w,t}$ detection, a flow of 6 l min^{-1} is sampled from the aerosol vessel through a stainless steel tube heated to temperatures above 20°C. Thus liquid aerosol and ice particles evaporate and contribute to $e_{w,t}$. Because the aerosol water content contributed only a negligible fraction to the total water concentration in all experiments discussed here (see section 2.4), $e_{w,t} \approx e_w$ before ice particles are formed. The ice saturation at the onset time t_{IN} of ice nucleation is therefore obtained from both the sampling and in situ water measurement as $S_{IN} = e_w(t_{IN})/e_{ice}(t_{IN}) = e_{w,t}(t_{IN})/e_{ice}(t_{IN})$. Measurements of t_{IN} will be described in the following section. The uncertainty of S_{IN} is about ±0.08 at the highest temperatures and ±0.13 at the lowest temperatures with major contributions from the temperature fluctuation of ±0.3 K and the uncertainty of about ±5 to ±10% for the water vapor concentration.

2.2. Ice Particle Measurements

[16] The onset time t_{IN} of ice formation is measured independently with two methods, (1) the increase of scattering and depolarization of polarized laser light and (2) the increase of the ice particle number concentration detected with an optical particle counter. The first method relies on the increase of the depolarization ratio of back-scattered argon ion laser light at 488 nm (detection angle of 176°) and an increase of the forward (detection angle 4°) and backward scattering intensity by growing ice crystals. The depolarization ratio and scattering intensities are measured with a time resolution of 1 s. For more details of the scattering measurements see *Möhler et al.* [2003]. The optical particle counter (OPC) situated below the aerosol vessel measures the number concentration and sizes of ice particles exceeding ∼1 μm in diameter in a strictly vertical sample flow of 5 l min^{-1}. For the experiments with soot particles, the OPC was sensitive to ice particle number concentrations of less than 1 cm^{-3}. Because the aerosol number concentration was larger than 300 cm^{-3} in all experiments with uncoated soot aerosol, the ice saturations at nucleation onset discussed in section 3.1 represent less than ∼0.3% of the soot aerosol particles acting as ice nuclei. After the deposition nucleation on the uncoated soot particle surface the ice phase grows by vapor deposition to the nm-sized critical nuclei. At a given supersaturation, the growth rate is decreasing with decreasing temperature. At temperatures below ∼195 K, t_{IN} is therefore corrected for the fact that pristine ice crystals need up to 20 s to grow to minimum sizes of ∼0.2 μm and 1.0 μm for detection with the depolarization method and the optical particle counter, respectively. This caused an increased uncertainty of S_{IN} at the lowest temperatures. This systematic time shift was estimated from the growth rate equation assuming spherical ice particles. For the experiments with sulfuric acid–coated soot particles, the threshold for determining t_{IN} was set to 5 cm^{-3} because of some scatter in the background concen-

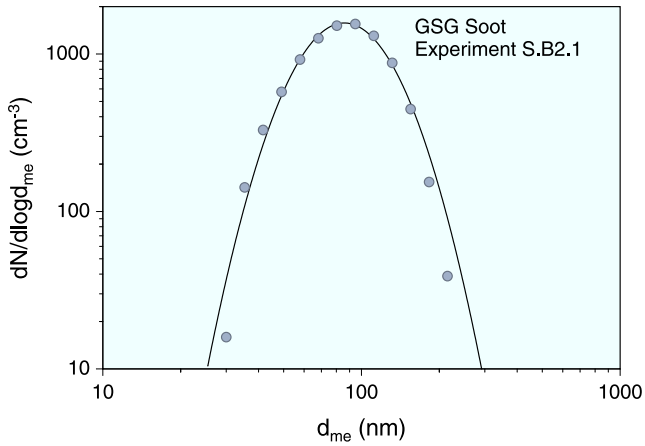

Figure 3. Number size distribution of uncoated GSG soot aerosol measured with the DMPS before experiment S.B2.1. The solid line shows the result of a lognormal fit to the measured distribution with a count median diameter of 90 nm and a geometric standard deviation of 1.47. The size distribution was similar in all experiments with pure soot aerosol.

tration from the larger aerosol size fraction. Again, with the somewhat higher aerosol number concentration during the coated soot experiments, the given ice nucleation thresholds are representative of less than 0.3% of the aerosol particles.

[17] In situ FTIR extinction measurements are sensitive to ice mass concentrations above 5 μg m^{-3}. A White-type multiple reflection cell with a maximum path length of 254.3 m [*Wagner et al.*, 2003] is used to measure FTIR extinction spectra of ice crystals in time steps of ∼20 s. The spectra are recorded with a Bruker IFS 66v FTIR spectrometer between 800 and 6000 cm^{-1} with a resolution of 4 cm^{-1}. Ice particle number concentrations are retrieved from the FTIR spectra using a method described by *Mangold et al.* [2005]. Results are shown in Figure 2 and are discussed in section 3.2.

2.3. Aerosol Generation and Characterization

[18] A commercial instrument (GfG1000), hereinafter referred to as Graphite Spark Generator (GSG), was used to generate soot aerosol in a 5 l min^{-1} argon flow by a spark discharge between pure graphite electrodes. The morphology, organic carbon to elemental carbon ratio, and optical properties of GSG soot were comprehensively analyzed in previous AIDA studies [*Saathoff et al.*, 2003; *Schnaiter et al.*, 2003]. Briefly, the soot aerosol size distributions measured with a differential mobility particle sizer (DMPS) can be approximated by a lognormal distribution. The example shown in Figure 3 has a median diameter of 90 nm and a geometric standard deviation of 1.47. Depending on the aerosol number concentration (about 300 to 5000 cm^{-3}) (see Table 1), the count median diameters ranged from 70 to 140 nm and the geometric standard deviations from 1.45 to 1.6. The fractal-like soot agglomerates are composed of primary particles with diameters between 4 and 8 nm. The GSG soot mainly contains elemental carbon (EC) analyzed by a thermal technique [*Verein Deutscher Ingenieure*, 1999] with ∼10% organic carbon (OC) content.

[19] GSG soot particles were coated with sulfuric acid in a system which is shown schematically in the bottom left area of Figure 1. Soot aerosol was mixed with a flow of synthetic air saturated with sulfuric acid vapor at a temperature between 320 K and 370 K. Sulfuric acid vapor

Table 1. Parameters of Individual AIDA Ice Activation Experiments With Uncoated GSG Soot Aerosol[a]

Experiment	p_0, hPa	$T_{g,0}$, K	t_{IN}, s	p_{IN}, hPa	$T_{g,IN}$, K	S_{IN}	$(dp/dt)_{IN}$, hPa min^{-1}	$(dT_g/dt)_{IN}$, K min^{-1}	$(dS_{ice}/dt)_{IN}$, min^{-1}	$C_{n,IN}$, cm^{-3}
S.A1.1	1017.1	195.7	58	964.8	193.0	1.29 ± 0.081	−50.1	−2.4	0.45	
S.A1.2	1016.9	195.6	57	966.7	193.1	1.28 ± 0.080	−49.3	−2.3	0.41	
S.A1.3	827.0	195.0	52	788.7	192.6	1.28 ± 0.081	−40.7	−2.4	0.45	
S.A2.1	1018.8	216.2	35	983.5	214.4	1.19 ± 0.068	−49.6	−2.8	0.38	
S.A2.2	1018.5	216.3	25	992.0	214.9	1.10 ± 0.066	−57.5	−3.4	0.43	
S.A2.4	1018.8	214.8	25	994.3	213.4	1.10 ± 0.067	−61.3	−3.5	0.44	
S.B1.1	1005.7	188.5	110	944.8	185.7	1.33 ± 0.13	−30.5	−1.3	0.21	2182
S.B1.2	1005.7	188.7	100	949.5	186.1	1.26 ± 0.13	−31.0	−1.3	0.21	1617
S.B1.3	1005.9	188.7	130	943.1	185.9	1.34 ± 0.13	−25.1	−0.9	0.14	1195
S.B2.1	997.9	239.5	130	920.4	235.2	1.29 ± 0.066	−30.5	−1.3	0.14	1384
S.B2.2	998.0	239.3	132	919.7	235.0	1.28 ± 0.066	−31.8	−1.3	0.14	1168
S.B2.3	998.0	239.3	198	886.8	233.7	1.29 ± 0.066	−28.3	−0.9	0.09	823
S.B2.4	1001.8	240.2	283	863.7	233.3	1.27 ± 0.066	−34.2	−1.3	0.14	566
S.B3.1	1000.7	245.1	207	882.3	239.2	1.33 ± 0.066	−28.3	−0.6	0.04	581
S.B3.2	1001.7	245.0	145	901.6	239.6	1.32 ± 0.065	−36.1	−1.1	0.11	422
S.B3.3	1001.7	245.1	155	895.8	239.3	1.34 ± 0.066	−35.3	−1.6	0.17	300
S.C1.1	1005.5	195.3	80	956.6	193.0	1.29 ± 0.081	−33.7	−1.3	0.24	812
S.C1.2	1005.4	195.6	80	957.4	193.2	1.30 ± 0.081	−32.9	−1.5	0.27	591
S.C1.3	1003.8	195.7	85	959.1	193.5	1.26 ± 0.080	−31.0	−1.2	0.20	430
S.C1.4	1002.9	195.8	80	959.7	193.6	1.30 ± 0.081	−29.7	−1.3	0.23	314
S.C2.1	1007.2	211.2	65	955.7	208.4	1.17 ± 0.071	−44.4	−2.3	0.33	1901
S.C2.3	1008.2	211.0	110	956.1	208.4	1.18 ± 0.071	−25.5	−1.0	0.13	1015
S.C2.4	1008.5	211.0	130	947.4	208.4	1.11 ± 0.069	−24.5	−0.6	0.07	747
S.C3.1	1006.0	226.0	40	971.7	224.0	1.15 ± 0.065	−50.3	−2.8	0.34	4881
S.C3.2	1006.4	226.0	44	968.9	223.8	1.16 ± 0.066	−49.6	−2.9	0.35	3599
S.C3.3	1006.3	226.0	120	964.7	223.7	1.16 ± 0.066	−28.1	−1.5	0.18	2701

[a]The pressure p_0 and temperature $T_{g,0}$ are almost constant until the reference time t_0 defined by the start of pumping. The onset time t_{IN} of ice nucleation is given in seconds relative to t_0. The following parameters are determined at t_{IN}: pressure p_{IN}, mean gas temperature $T_{g,IN}$, ice saturation ratio S_{IN}, pressure change $(dp/dt)_{IN}$, cooling rate $(dT_g/dt)_{IN}$, and aerosol number concentration $C_{n,IN}$.

condensed onto the soot particles upon cooling of the saturated mixture in a temperature gradient flow tube. The nucleation of pure sulfuric acid droplets was suppressed by properly adjusting the flow rates and the cooling profile. The sulfuric acid–coated (SAC) soot aerosol was then added to the aerosol chamber. Measurements of the total sulfuric acid mass concentration of the coated aerosol are discussed in section 2.4.

[20] Figure 4 shows a typical size distribution of SAC soot in the AIDA chamber which can be approximated by a lognormal size distribution. Because of the sulfuric acid layer the median diameter is somewhat larger (140 nm) compared to the pure GSG soot aerosol shown in Figure 3. Because the fractal soot aggregates shrink during the coating process, the geometric standard deviation is only 1.29 for the SAC soot compared to 1.47 for the GSG soot aerosol.

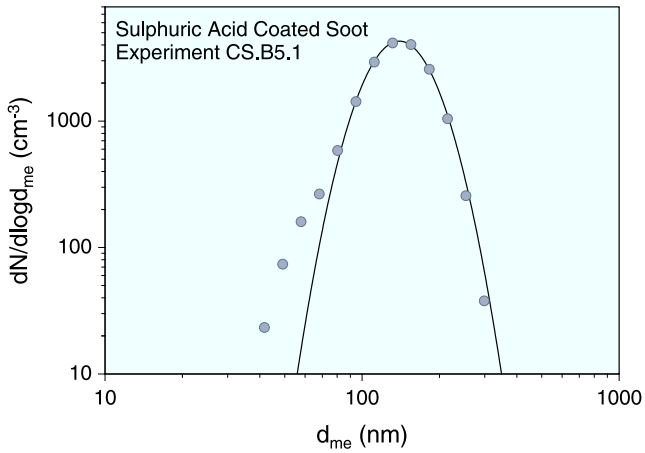

Figure 4. Same as Figure 3 but for soot coated with sulfuric acid added to the aerosol chamber before experiment CS.B5.1. The lognormal fit to the measured distribution reveals a count median diameter of 140 nm and a standard deviation of only 1.29. The total aerosol volume is 5.0 μm^3 cm^{-3}, and the sulfuric acid volume, measured by ion chromatographic analysis of filter samples, is 3.9 μm^3 cm^{-3}.

2.4. Experimental Parameters

[21] Three series of ice nucleation experiments, labeled "A," "B," and "C" in Table 1, were carried out with uncoated GSG soot. The gas temperature $T_{g,0}$ before starting an expansion varied from 189 K in experiment B1 to 245 K in experiment B3. After the first expansion from about 1000 to 800 hPa, the chamber was replenished with particle-free, dry synthetic air to the starting pressure p_0 of the subsequent expansion with the same aerosol. Thereby, the gas temperature increased by ~5 K, the relative humidity with respect to ice dropped below 50%, and all ice crystals from the preceding ice activation evaporated. Series of up to 4 ice activations were made with the same aerosol and at almost identical $T_{g,0}$ in order to investigate possible cloud processing effects. The aerosol number concentrations $C_{n,IN}$ (the subscript IN refers to the freezing onset time t_{IN} as detailed in section 2.2) during ice nucleation ranged from about 300 to 5000 cm^{-3}. In consecutive ice activations of the same aerosol, the number concentrations decreased each time ~20% by dilution. Additional losses may occur because of sedimentation of larger ice crystals, especially during experiments at higher temperatures where more water is available for ice crystal growth.

[22] The pumping speed was also systematically varied in repeated ice activation experiments to investigate the impact of the cooling rate dT_g/dt or the respective rate of ice saturation increase dS_{ice}/dt on the formation rate of ice crystals and the ice microphysics. An example will be discussed in section 3.2. The cooling rates $(dT_g/dt)_{IN}$ at freezing onset, also given in Table 1, ranged from −0.6 to −3.5 K min^{-1}. As mentioned in section 2.1, dT_g/dt and dS_{ice}/dt not only depend on the pumping speed but also on heat and water fluxes from the ice-coated vessel walls. $(dS_{ice}/dt)_{IN}$ listed in Table 1 was calculated from equation (3) neglecting the water flux from the vessel walls. This is a good approximation until the water vapor drops because of crystal growth after the ice nucleation onset. The effects of heat and water vapor fluxes must, however, be taken into account when using a process model to interpret the experimental results in terms of quantitative nucleation rates. In this paper we limit our discussion to the critical ice saturation ratios S_{IN} (section 3.1) and a case study on the formation rate of ice crystals at different cooling rates and ice nucleation modes (section 3.2). The aspects of nucleation rates and crystal growth will be in the focus of further process modeling studies.

[23] The ice nucleation by SAC soot was investigated in another series of 14 experiments started at temperatures between 188 K and 236 K (see Table 2). As for the uncoated soot experiments, pumping started at ~1000 hPa. In most cases, two consecutive activations were carried out with the same aerosol, as described previously. The cooling rates $(dT_g/dt)_{IN}$ varied between −0.8 and −3.6 K min^{-1}, while $(dS_{ice}/dt)_{IN}$ calculated using equation (3) ranged from 0.16 min^{-1} to 0.61 min^{-1}. With values between 2500 and 56,000 cm^{-3}, the aerosol number concentrations were up to 10 times higher than during the experiments with uncoated soot aerosol. The aerosol sulfate mass concentration $C_{m,sulfate}$ in the AIDA chamber, obtained from ion chromatographic analysis of nylon filter samples, varied from about 1 to 74 $\mu g\ m^{-3}$ as summarized in Table 3.

[24] The SAC soot particles were transferred to the AIDA aerosol vessel in a synthetic air flow at low relative humidities, i.e., high concentrations of sulfuric acid in the coating layer. In the AIDA vessel, the particles quickly take up water vapor until thermodynamic equilibrium is established according to the AIDA temperature and relative humidity conditions. As shown in Table 3, the sulfuric acid weight fraction w_{SA} at ice saturation varies from 38% at 188 K to 30% at 236 K. To estimate the mean volume fraction $f_{v,SA}$ of the coating layer to the total aerosol volume, the sulfuric acid volume concentration $C_{v,SA}$ was calculated from $C_{m,sulfate}$, measured by ion chromatographic analysis of filter samples, and w_{SA}, assuming a density of 1.4 g cm^{-3} for the supercooled aqueous sulfuric acid (see Table 3). During filter sampling, the number size distribution of the same aerosol was measured with a DMPS (see Figures 3 and 4 in section 2.3). This system was especially modified and designed for measurements at low temperatures [*Seifert et al.*, 2004]. It measures the size distributions at very close to

Table 2. Parameters of Individual AIDA Ice Activation Experiments With SAC Soot Aerosol[a]

Experiment	p_0, hPa	$T_{g,0}$, K	t_{IN}, s	p_{IN}, hPa	$T_{g,IN}$, K	S_{IN}	$(dp/dt)_{IN}$, hPa min^{-1}	$(dT_g/dt)_{IN}$, K min^{-1}	$(dS_{ice}/dt)_{IN}$, min^{-1}	$C_{n,IN}$, cm^{-3}
CS.B1.1	1,001.8	188.4	160	927.2	185.2	1.48 ± 0.100	−25.7	−0.8	0.16	7,654
CS.B1.2	1,001.8	188.5	100	941.7	185.7	1.55 ± 0.100	−33.0	−1.5	0.32	5,635
CS.B2.1	999.8	200.2	89	952.2	197.9	1.35 ± 0.081	−27.7	−1.3	0.23	17,734
CS.B2.2	999.8	200.1	100	935.7	197.0	1.50 ± 0.087	−34.2	−1.7	0.35	12,265
CS.B3.1	1,010.9	206.0	150	913.8	201.4	1.43 ± 0.082	−33.6	−1.3	0.22	56,140
CS.B3.2	1,011.4	206.2	110	921.6	201.7	1.43 ± 0.082	−44.2	−1.9	0.34	38,363
CS.B4.1	1,012.8	207.6	90	937.9	203.7	1.43 ± 0.081	−46.1	−2.0	0.35	41,664
CS.B5.1	1,019.8	211.9	60	967.2	209.0	1.32 ± 0.078	−49.8	−2.5	0.42	3,478
CS.B5.2	999.6	211.9	50	956.5	209.4	1.28 ± 0.076	−49.2	−2.8	0.47	2,533
CS.B5.3	998.8	211.9	40	956.3	209.4	1.29 ± 0.077	−62.9	−3.6	0.61	1,970
CS.B6.1	999.5	225.0	70	936.7	221.3	1.34 ± 0.071	−48.9	−2.7	0.38	3,989
CS.B6.2	997.3	225.0	60	943.4	221.9	1.23 ± 0.068	−50.2	−2.5	0.32	2,867
CS.B7.1	1,008.8	234.6	80	935.3	230.2	1.26 ± 0.067	−52.7	−2.8	0.34	31,263
CS.B8.2	1,003.3	236.1	80	930.1	231.7	1.41 ± 0.069	−49.8	−2.7	0.36	5,760

[a]See Table 1 for a description of abbreviations and symbols.

chamber conditions with respect to temperatures and humidities. The number concentrations $C_{n,ae}$, mean diameters d_n, and geometric standard deviations σ_n of lognormal fits to the DMPS size distributions are listed in Table 3. The volume concentration $C_{v,ae}$ of the SAC aerosol was calculated from these lognormal fits. Finally, the volume fraction $f_{v,SA}$ of the sulfuric acid coating is given by the ratio $C_{v,SA}/C_{v,ae}$. Table 3 shows the coated aerosol to contain significant amounts of sulfuric acid with volume fractions between 0.21 and 0.81.

3. Results and Discussion

3.1. Nucleation Onset

[25] Figure 5 shows critical ice saturation ratios S_{IN} measured at the onset time t_{IN} of ice nucleation as function of the temperature T_{IN} for all ice nucleation experiments with uncoated GSG soot. As mentioned in section 2.2, the S_{IN} data discussed in this paper represent less than ∼0.3% of the respective aerosol particles acting as ice nuclei. Clusters of up to four data points at almost the same temperature (see Table 2) belong to consecutive activations of the same aerosol that are distinguished by different symbols. Within the given uncertainties, there is no significant trend in S_{IN} in consecutive activations. However, S_{IN} significantly varies with temperature. The lowest IN thresholds in terms of S_{ice} are measured at intermediate temperatures around 210 K. With decreasing temperature, S_{IN} increases to ∼1.3 at the lowest ice nucleation temperature of ∼186 K. At temperatures between 235 K and 240 K, S_{IN} approaches the supercooled water saturation limit indicated by the dashed line in Figure 5. Here, ice seems to form immediately after liquid activation of the soot particles either by condensation freezing or homogeneous freezing of the growing liquid water layer, depending on the actual temperature of the water condensation layer. Note that, at temperatures below 235 K, the critical saturation ratios are always markedly lower than the threshold values for homogeneous freezing of solution droplets [*Koop et al.*, 2000] indicated by the solid line in Figure 5. This line was calculated for $\Delta a = 0.303$ which corresponds to a nucleation rate of $1.9 \cdot 10^9$ cm^{-3} s^{-1}. The low ice nucleation threshold indicates the soot particles to act as efficient deposition nuclei at cirrus temperatures.

[26] The ice nucleation thresholds S_{IN} measured for SAC soot particles are shown in Figure 6. As for the uncoated soot aerosol, there is no significant trend of S_{IN} in consecutive ice activations of the same aerosol that are also distinguished by different symbols in Figure 6. In general, S_{IN} of SAC soot increases from ∼1.3 at 230 K to ∼1.5 at 185 K, which corresponds to a negative offset of roughly 0.15 below the homogeneous freezing thresholds of supercooled solution droplets represented by the same solid line as in Figure 5. Previous results by *DeMott et al.* [1999] for redispersed Degussa soot with monolayer and multilayer sulfuric acid coatings are also shown in Figure 6. The soot

Table 3. Aerosol Volume Fraction of the Sulfuric Acid Coating on the Soot Particles Calculated From the Ratio of the Volumetric Aerosol Sulfuric Acid Content and the Total Aerosol Volume[a]

Experiment	$T_{g,0}$, K	$C_{m,sulfate}$, μg m^{-3}	w_{SA}, wt.%	$C_{v,SA}$, μm^{3}cm^{-3}	$C_{n,ae}$, cm^{-3}	d_n, μm	σ_n	$C_{v,ae}$, μm^{3}cm^{-3}	$f_{v,SA}$
CS.B1.1	188.4	1.1 ± 0.3	38	2.1 ± 0.6	9,000	0.09	1.36	5.3 ± 1.6	0.40 ± 0.16
CS.B2.1	200.2	1.6 ± 0.5	37	3.1 ± 0.9	21,000	0.10	1.38	15.0 ± 4.5	0.21 ± 0.08
CS.B4.1	207.6	36.7 ± 0.4	36	73 ± 0.7	75,000	0.17	1.33	280 ± 84	0.26 ± 0.08
CS.B5.1	211.9	1.9 ± 0.6	35	3.9 ± 1.2	2,700	0.14	1.29	5.0 ± 1.5	0.78 ± 0.33
CS.B6.1	225.0	2.4 ± 0.7	33	5.2 ± 1.6	3,500	0.15	1.26	7.2 ± 2.2	0.72 ± 0.30
CS.B7.1	234.6	73.6 ± 0.7	31	170 ± 1.7	40,000	0.20	1.25	211 ± 63	0.81 ± 0.26
CS.B8.2	236.1	3.9 ± 1.1	30	9.3 ± 2.0	7,000	0.14	1.28	13.0 ± 4.9	0.72 ± 0.30

[a]Total aerosol volume was calculated from lognormal fits to the measured aerosol size distributions. Only one filter sample was taken for each day of subsequent experiments, either before or after the first expansion. For further parameters of these experiments, see Table 2. Abbreviations are as follows: $T_{g,0}$, gas temperature; $C_{m,sulfate}$, aerosol sulfate mass concentration; w_{SA}, sulfuric acid mass fraction at ice saturation; $C_{v,SA}$, total volume concentration of aqueous sulfuric acid, calculated from $C_{m,sulfate}$ and w_{SA} with a density of 1.4 g cm^{-3}; $C_{n,ae}$, total aerosol number concentration; d_n, median diameter; $\sigma_{g,n}$, geometric standard deviation of the lognormal fit to the measured aerosol number size distributions; $C_{v,ae}$, total aerosol volume concentrations calculated from the lognormal fit; $f_{v,SA} = C_{v,SA}/C_{v,ae}$, mean sulfuric acid volume fraction of the aerosol particles during experiments with sulfuric acid–coated soot.

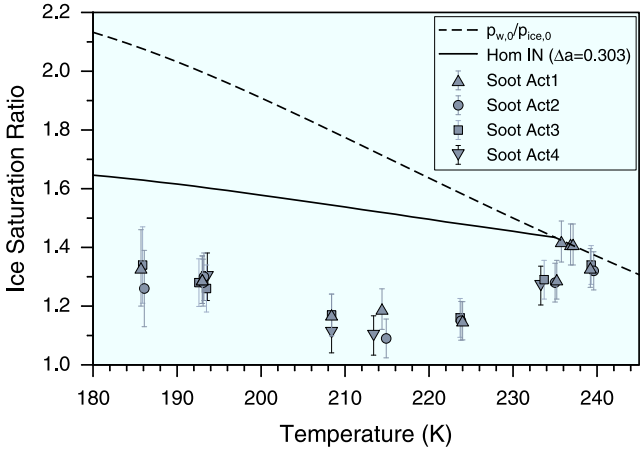

Figure 5. Ice saturation at freezing onset measured for uncoated GSG soot aerosol (data from Table 1). The different symbols show results of repeated activations with the same soot aerosol in the aerosol chamber. The aerosol chamber was refilled with particle-free synthetic air after each activation. For comparison, the homogeneous freezing threshold of supercooled solution droplets [*Koop et al.*, 2000] is indicated by the solid line. Water saturated conditions are indicated by the dashed line. The water saturation pressure was taken from a parameterization given by *Tabazadeh et al.* [1997] which may be uncertain by more than 10% at temperatures below 190 K.

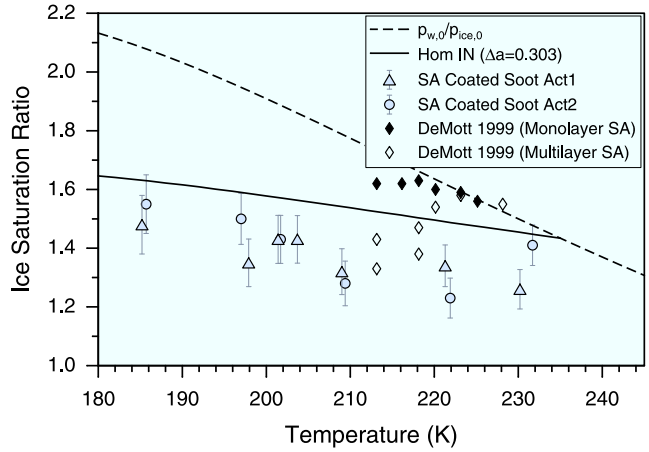

Figure 6. Ice saturation measured at freezing onset of SAC soot particles (data from Table 2). First and second activations of the same aerosol in the aerosol chamber are indicated by triangles and circles, respectively. The AIDA data are compared to freezing relative humidities measured by *DeMott et al.* [1999] for redispersed Degussa soot with monolayer or multilayer sulfuric acid coating. For comparison, the homogeneous freezing threshold of supercooled solution droplets [*Koop et al.*, 2000] is indicated by the solid line. Water saturated conditions are indicated by the dashed line [*Tabazadeh et al.*, 1997].

aerosol used in that study was generated by dispersing a sample of dry carbon particles (lamp black) from Degussa Corporation (Frankfurt, Germany). The aerosol with aggregate-like black carbon particles could also be approximated by a lognormal size distribution with number concentrations up to 2000 cm^{-3}, in the range of concentrations used in our experiments, but somewhat larger mean diameter of 240 nm and geometric standard deviation of 1.6. The Degussa black carbon particles with monolayer sulfuric acid coating (Figure 6, solid diamonds) nucleated ice only at high ice saturation ratios close to the homogeneous freezing threshold expected for pure sulfuric acid particles of similar volume as the coating layer on the soot particles. Only multilayer coating of Degussa soot with sulfuric acid shifted the ice nucleation threshold to lower values (Figure 6, open diamonds), well into the range where SAC GSG soot formed ice particles.

[27] *DeMott et al.* [1999] also investigated uncoated Degussa soot particles which acted as deposition or sorption nuclei near but still below water saturation. In contrast, uncoated GSG soot particles are far more efficient deposition nuclei at temperatures below 235 K (see Figure 5). This marked difference cannot be explained by a simple size effect. A more likely explanation could be different surface properties and/or other relevant characteristics (porosity, surface area, organic carbon content) of the GSG and Degussa soot aerosols. For the Degussa soot the manufacturer quoted a BET surface area of 20 m^2g^{-1} [*DeMott et al.*, 1999]. Thermodesorption of nitrogen was employed by *Kuznetsov et al.* [2003] to determine the specific surface area of GSG soot to 308 ± 30 m^2g^{-1}. For this analysis the GSG soot was directly collected from the spark discharge generator of the AIDA facility.

[28] Coating GSG soot particles with sulfuric acid affects both the mechanism and saturation threshold for ice nucleation. Figure 7 directly compares S_{IN} measured for both uncoated GSG (triangles) and SAC (diamonds) soot particles. Previous AIDA results for the homogeneous freezing of pure sulfuric acid solution droplets [*Möhler et al.*, 2003] are also shown (circles). In the entire temperature range from 185 K to 220 K, the internal mixture of soot and sulfuric acid nucleates ice at S_{IN} between that of pure GSG

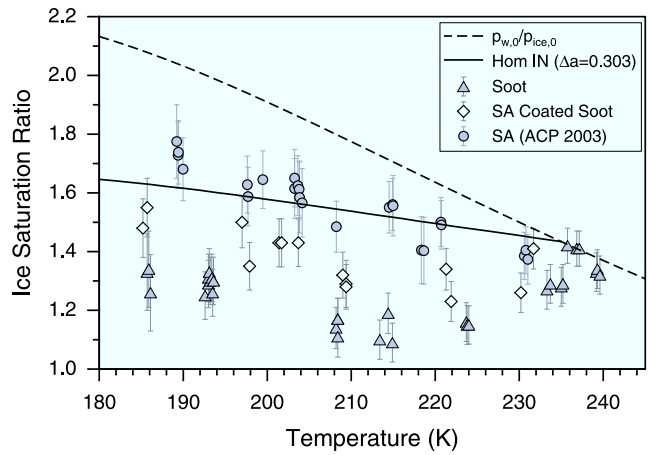

Figure 7. Ice saturation measured at freezing onset of uncoated GSG soot particles, sulfuric acid (SA)–coated soot, and pure sulfuric acid solution droplets adopted from *Möhler et al.* [2003]. For comparison, the homogeneous freezing threshold of supercooled solution droplets [*Koop et al.*, 2000] is indicated by the solid line. Water saturated conditions are indicated by the dashed line [*Tabazadeh et al.*, 1997].

soot and pure sulfuric acid particles. If ice nucleation of SAC soot occurred because of purely homogeneous freezing of the sulfuric acid coating, ice nucleation should occur at S_{IN} comparable to or slightly higher than (in view of the smaller liquid volume of the coating layer) the nucleation thresholds which have been determined in the AIDA facility for pure sulfuric acid aerosol (Figure 7, circles) [*Möhler et al.*, 2003]. This indicates that the liquid coating undergoes immersion freezing which shifts the nucleation threshold below the homogeneous nucleation threshold of the pure sulfuric acid solution.

3.2. Formation Rate of Ice Particles

[29] Figure 2 (fifth panel) shows time series of ice particle number concentrations, n_{ice}, measured directly with the optical particle counter (solid line) or retrieved from FTIR extinction spectra (solid symbols). Both data sets agree within experimental errors. After nucleation onset indicated by the vertical line, n_{ice} steadily increases with a slow rate of $\sim$0.4 cm^{-3} s^{-1}. Because the few ice crystals take up only a minor fraction of the available water vapor, the ice saturation also continues to increase after the nucleation onset to a maximum value close to 1.6, which is slightly below the homogeneous freezing threshold for small solution droplets at the respective temperature of $\sim$205 K. No second peak of homogeneously freezing sulfuric acid occurred during this expansion. The steady increase of the ice particle number concentration indicates that for the immersion freezing of sulfuric acid solution in contact with the soot surface there is only a weak dependence of the ice formation rate, i.e., the nucleation rate, on increasing S_{ice} and thereby on the increasing water content of the sulfuric acid solution. Interestingly, n_{ice} continued to increase even after S_{ice} passed its maximum value and started to decrease already. This behavior also indicates a very low nucleation rate or some other, possibly time-dependent mechanism we cannot fully understand on the basis of the experimental data set we have so far. On the other hand, the immersion freezing mechanism could also be described in terms of specific surface sites that are activated at different S_{ice} and temperatures. In this case additional sites may be activated because of the steadily decreasing temperature until pumping stops and the ice number concentration reaches its maximum. Note that only $\sim$3% of the aerosol particles nucleated ice in this experiment.

[30] This is somewhat different to experiment CS.B5.3 which showed two distinct nucleation peaks. This experiment followed CS.B5.2 discussed above, with still the same aerosol but at a somewhat higher cooling rate. Time series of the experimental data are shown in Figure 8. Figure 8 (fifth panel) again depicts n_{ice} measured with the optical particle counter. No FTIR spectra are available for this experiment. As during experiment CS.B5.2, a few ice crystals are formed by immersion freezing at a relatively low saturation ratio. The onset of immersion freezing is indicated by the dashed vertical line.

[31] However, for the higher cooling rate of experiment CS.B5.3, the formation rate of ice crystals by heterogeneous freezing and their mass growth rate are not high enough to limit the peak relative humidity to a value below the homogeneous freezing threshold. The cooling rate was -3.6 K min^{-1} at the immersion freezing onset compared

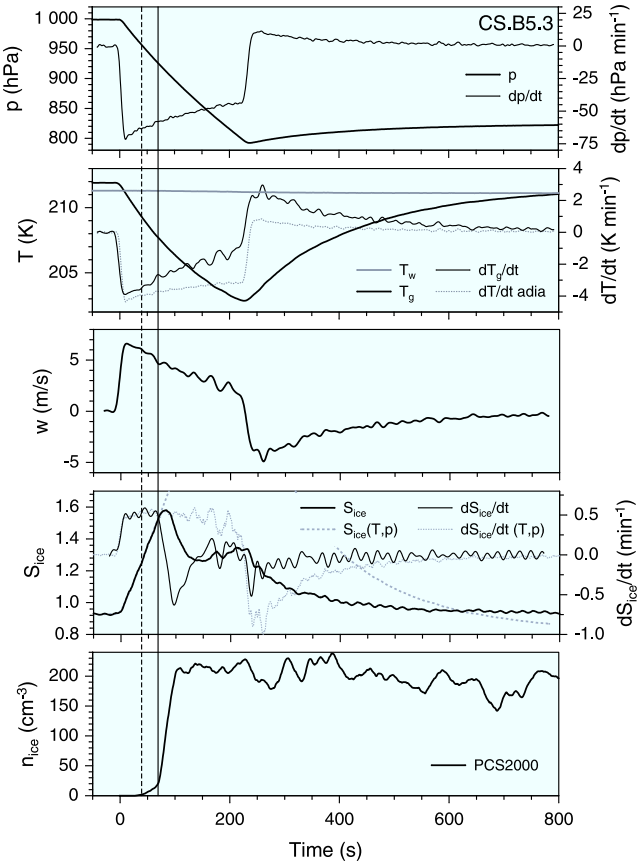

Figure 8. Same as Figure 2 but for the subsequent activation CS.B5.3 of the same aerosol with higher pumping speed and therefore higher rates of cooling and ice saturation increase. A second mode of homogeneous freezing of the sulfuric acid layer, indicated by the solid vertical line, occurs after the formation of fewer ice particles due to heterogeneous ice nucleation at lower S_{ice}.

to -2.8 K min^{-1} for the previous expansion (see also Table 2). The corresponding increase of the ice saturation ratio was 0.61 min^{-1} and 0.47 min^{-1}, respectively. Therefore, as S_{ice} approaches a value of $\sim$1.6, n_{ice} steeply increases indicated by the solid vertical line in Figure 8. This may be explained by homogeneous freezing of the sulfuric acid layer around the soot particles. A number of 200 cm^{-3} ice particles is nucleated within a short time period, growing by water uptake and thereby limiting S_{ice} to a peak value only slightly above the onset value for homogeneous freezing. A similar temporal behavior of n_{ice} and S_{ice} was also observed in previous homogeneous freezing experiments with pure sulfuric acid aerosols [*Möhler et al.*, 2003] and was consistently explained with detailed process modeling [*Haag et al.*, 2003a].

[32] A detailed comparison of the heterogeneous and homogeneous ice nucleation rates may be achieved with a detailed process modeling study which is beyond the scope of the present paper but is part of ongoing work. On the other hand, the case study we have discussed for experiments CS.B5.a and CS.B5.3 with fully internally mixed soot and sulfuric acid particles, indicate that, in contrast to homogeneous freezing, immersion freezing induces a some-

what broader nucleation peak as function of temperature and ice supersaturation. This may be explained by a limited fraction of soot particles with surface sites which are activated at a given temperature and ice supersaturation.

4. Summary and Conclusions

[33] The critical saturation ratios for ice nucleation of uncoated graphite spark generator (GSG) soot and sulfuric acid–coated (SAC) GSG soot were investigated at temperatures between 186 K and 240 K. The ice initiation was achieved in dynamic expansion experiments simulating cloud cooling rates between about -0.6 and -3.6 K min^{-1}. In three series of experiments with GSG soot consisting of fractal agglomerates with very large specific surface area of 308 ± 30 m^{2}g^{-1} [*Kuznetsov et al.*, 2003] and ~10% organic carbon (OC), ice nucleation occurred after the ice saturation exceeded values of ~1.3 at 186 K, a minimum of ~1.1 at about 210 K, and ~1.4 at 240 K, which is close to liquid water saturation at this temperature. From this we conclude that in the mixed cloud regime soot particles only act as freezing nuclei after liquid droplet activation. This is in agreement with a previous study by *DeMott* [1990] using flame soot particles. In contrast to our results at lower temperatures *DeMott et al.* [1999] have found that uncoated Degussa soot particles acted as deposition or sorption nuclei only at very high ice supersaturations near but still below water saturation. This marked difference may be attributed not only to the much smaller specific surface area of 20 m^{2}g^{-1} but also to different physical or chemical surface characteristics of both soot samples. On the basis of our laboratory study we are not able to decide which soot is more relevant to the atmosphere. On the other hand, the results indicate that the ice nucleating behavior of pure soot particles, if present in the atmosphere, may markedly depend on their physical and chemical properties. This conclusion is also supported by recent results from further AIDA ice nucleation experiments with flame soot indicating significant suppression of ice nucleation efficiency with increasing organic carbon content of the soot aerosol [*Möhler et al.*, 2005].

[34] Another factor significantly changing the ice nucleation thresholds of GSG soot is coating with sulfuric acid. The results discussed in this paper clearly show that coating with sulfuric acid layers contributing between 21 and 81% to the total aerosol volume increased the ice saturation ratios required for ice nucleation by GSG soot by about 0.1 to 0.3 at temperatures below 232 K. The measured ice nucleation thresholds are still lower than those measured for pure sulfuric acid droplets with the same method [*Möhler et al.*, 2003]. Therefore soot particles have a significant heterogeneous freezing effect on the ice nucleation of supercooled sulfuric acid solutions lowering the threshold relative humidities required for ice nucleation by ~10% at 230 K and 20% at 185 K. This seems to be in conflict with a previous study by *DeMott et al.* [1999] where they showed that the freezing threshold of Degussa soot particles was lowered when the particles were coated with sulfuric acid. Uncoated Degussa soot seems to be a very poor substrate for ice nucleation, whereas GSG soot particles are fairly efficient deposition freezing nuclei. The results of our work show furthermore that the mixing state of soot particles with sulfuric acid affects the threshold relative humidity of ice nucleation in the whole temperature range of cirrus formation. The lower immersion freezing thresholds of the internally mixed soot and sulfuric acid particles are close to those found for dust particles immersed in ammonium sulfate particles [*Zuberi et al.*, 2002; *Hung et al.*, 2003].

[35] Considering ice nucleation in cloud and climate models not only needs ice nucleation onset thresholds but also parameterizations for the ice particle number concentrations nucleating as a function of, e.g., temperature and ice saturation ratio. Concepts developed for the homogeneous freezing mode [*Kärcher and Lohmann*, 2002b] have recently been improved and applied for immersion freezing [*Kärcher and Lohmann*, 2003]. Similar to the homogeneous freezing, this concept also describes the nucleation rate basically as function of the temperature and ice saturation ratio, but additionally accounts for the freezing onset shifted to lower S_{ice}. Our results for the soot particles immersed in sulfuric acid clearly show a shift of the freezing onset to lower S_{ice}. A case study of two experiments with the same aerosol but different cooling rates showed that the formation rate of ice crystals as function of increasing ice saturation ratio is markedly lower for the immersion freezing mode than for the homogeneous freezing mode. Detailed process modeling studies may show if the experimental results discussed here can be explained within the theoretical framework for heterogeneous freezing developed by *Kärcher and Lohmann* [2003]. Further AIDA studies are underway measuring both the freezing onset and the ice particle concentration as function of the ice saturation ratio. The AIDA data sets will be used in further process modeling studies to validate existing or develop new concepts for parameterizing heterogeneous ice nucleation processes.

[36] **Acknowledgments.** We gratefully acknowledge skillful technical assistance by Rainer Buschbacher, Tomasz Chudy, Meinhard Koyro, Georg Scheurig, and Steffen Vogt in reliably running the AIDA facility during the ice nucleation experiments. We also thank Elisabeth Kranz for chemical analysis of filter samples. This work contributed to the HGF (Hermann von Helmholtz-Gemeinschaft Deutscher Forschungszentren) project Particles and Cirrus Clouds (PAZI).

References

Anderson, B. E., W. R. Cofer, D. R. Bagwell, J. W. Barrick, C. H. Hudgins, and K. E. Brunke (1998), Airborne observations of aircraft aerosol emissions I: Total nonvolatile particle emission indices, *Geophys. Res. Lett.*, *25*(10), 1689–1692.

Andronache, C., and W. L. Chameides (1997), Interactions between sulfur and soot emissions from aircraft and their role in contrail formation: 1. Nucleation, *J. Geophys. Res.*, *102*(D17), 21,443–21,451.

Chen, Y. L., S. M. Kreidenweis, L. M. McInnes, D. C. Rogers, and P. J. DeMott (1998), Single particle analyses of ice nucleating aerosols in the upper troposphere and lower stratosphere, *Geophys. Res. Lett.*, *25*(9), 1391–1394.

Curtius, J., F. Arnold, and P. Schulte (2002), Sulfuric acid measurements in the exhaust plume of a jet aircraft in flight: Implications for the sulfuric acid formation efficiency, *Geophys. Res. Lett.*, *29*(7), 1113, doi:10.1029/2001GL013813.

Cziczo, D. J., D. M. Murphy, P. K. Hudson, and D. S. Thomson (2004), Single particle measurements of the chemical composition of cirrus ice residue during Crystal-FACE, *J. Geophys. Res.*, *109*, D04201, doi:10.1029/2003JD004032.

DeMott, P. J. (1990), An exploratory study of ice nucleation by soot aerosols, *J. Appl. Meteorol.*, *29*(10), 1072–1079.

DeMott, P. J., Y. Chen, S. M. Kreidenweis, D. C. Rogers, and D. E. Sherman (1999), Ice formation by black carbon particles, *Geophys. Res. Lett.*, *26*(16), 2429–2432.

Ferry, G. V., et al. (1999), Effects of aircraft on aerosol abundance in the upper troposphere, *Geophys. Res. Lett.*, *26*(15), 2399–2402.

Field, P. R., et al. (2001), Ice nucleation in orographic wave clouds: Measurements made during INTACC, *Q. J. R. Meteorol. Soc.*, *127*(575), 1493–1512.

Gurlit, W., R. Zimmermann, C. Giesemann, T. Fernholz, V. Ebert, J. Wolfrum, U. Platt, and J. P. Burrows (2005), Lightweight diode laser spectrometer CHILD (Compact High-altitude In-situ Laser Diode) for balloonborne measurements of water vapor and methane, *Appl. Opt.*, *44*(1), 91–102.

Haag, W., B. Kärcher, S. Schaefers, O. Stetzer, O. Möhler, U. Schurath, M. Krämer, and C. Schiller (2003a), Numerical simulations of homogeneous freezing processes in the aerosol chamber AIDA, *Atmos. Chem. Phys.*, *3*, 195–210.

Haag, W., B. Kärcher, J. Ström, A. Minikin, U. Lohmann, J. Ovarlez, and A. Stohl (2003b), Freezing thresholds and cirrus cloud formation mechanisms inferred from in situ measurements of relative humidity, *Atmos. Chem. Phys.*, *3*, 1791–1806.

Hagen, D., P. Whitefield, J. Paladino, M. Trueblood, and H. Lilenfeld (1998), Particulate sizing and emission indices for a jet engine exhaust sampled at cruise, *Geophys. Res. Lett.*, *25*(10), 1681–1684.

Heymsfield, A. J., and L. M. Miloshevich (1993), Homogeneous ice nucleation and supercooled liquid water in orographic wave clouds, *J. Atmos. Sci.*, *50*(15), 2335–2353.

Heymsfield, A. J., and R. M. Sabin (1989), Cirrus crystal nucleation by homogeneous freezing of solution droplets, *J. Atmos. Sci.*, *46*(14), 2252–2264.

Hitzenberger, R., H. Giebl, A. Petzold, M. Gysel, S. Nyeki, E. Weingartner, U. Baltensperger, and C. W. Wilson (2003), Properties of jet engine combustion particles during the PartEmis experiment. Hygroscopic growth at supersaturated conditions, *Geophys. Res. Lett.*, *30*(14), 1779, doi:10.1029/2003GL017294.

Hung, H.-M., S. T. Malinowski, and S. T. Martin (2003), Kinetics of heterogeneous ice nucleation on the surfaces of mineral dust cores inserted into aqueous ammonium sulfate particles, *J. Phys. Chem. A*, *107*, 1296–1306.

Jensen, E. J., and O. B. Toon (1992), The potential effects of volcanic aerosols on cirrus cloud microphysics, *Geophys. Res. Lett.*, *19*(17), 1759–1762.

Jensen, E. J., and O. B. Toon (1997), The potential impact of soot particles from aircraft exhaust on cirrus clouds, *Geophys. Res. Lett.*, *24*(3), 249–252.

Jensen, E. J., et al. (1998), Ice nucleation processes in upper tropospheric wave-clouds observed during success, *Geophys. Res. Lett.*, *25*(9), 1363–1366.

Kärcher, B. (1998a), Physicochemistry of aircraft-generated liquid aerosols, soot, and ice particles: 1. Model description, *J. Geophys. Res.*, *103*(D14), 17,111–17,128.

Kärcher, B. (1998b), On the potential importance of sulfur-induced activation of soot particles in nascent jet aircraft exhaust plumes, *Atmos. Res.*, *46*(3–4), 293–305.

Kärcher, B., and U. Lohmann (2002a), A parameterization of cirrus cloud formation: Homogeneous freezing of supercooled aerosols, *J. Geophys. Res.*, *107*(D2), 4010, doi:10.1029/2001JD000470.

Kärcher, B., and U. Lohmann (2002b), A parameterization of cirrus cloud formation: Homogeneous freezing including effects of aerosol size, *J. Geophys. Res.*, *107*(D23), 4698, doi:10.1029/2001JD001429.

Kärcher, B., and U. Lohmann (2003), A parameterization of cirrus cloud formation: Heterogeneous freezing, *J. Geophys. Res.*, *108*(D14), 4402, doi:10.1029/2002JD003220.

Kärcher, B., and J. Ström (2003), The roles of dynamical variability and aerosols in cirrus cloud formation, *Atmos. Chem. Phys.*, *3*, 823–838.

Koop, T., B. P. Luo, A. Tsias, and T. Peter (2000), Water activity as the determinant for homogeneous ice nucleation in aqueous solutions, *Nature*, *406*(6796), 611–614.

Kristensson, A., J. F. Gayet, J. Ström, and F. Auriol (2000), In situ observations of a reduction in effective crystal diameter in cirrus clouds near flight corridors, *Geophys. Res. Lett.*, *27*(5), 681–684.

Kuznetsov, B. V., T. A. Rakhmanova, O. B. Popovicheva, and N. K. Shonija (2003), Water adsorption and energetic properties of spark discharge soot: Specific features of hydrophilicity, *J. Aerosol Sci.*, *34*(10), 1465–1479.

Lohmann, U., and B. Kärcher (2002), First interactive simulations of cirrus clouds formed by homogeneous freezing in the ECHAM general circulation model, *J. Geophys. Res.*, *107*(D10), 4105, doi:10.1029/2001JD000767.

Mangold, A., R. Wagner, H. Saathoff, U. Schurath, C. Giesemann, V. Ebert, M. Krämer, and O. Möhler (2005), Microphysics of cirrus clouds formed by different types of aerosols: experimental investigation in the aerosol chamber aida, *Meteorol. Z.*, in press.

Marti, J., and K. Mauersberger (1993), A survey and new measurements of ice vapor-pressure at temperatures between 170 and 250 K, *Geophys. Res. Lett.*, *20*(5), 363–366.

Miake-Lye, R. C., et al. (1998), SO_x oxidation and volatile aerosol in aircraft exhaust plumes depend on fuel sulfur content, *Geophys. Res. Lett.*, *25*(10), 1677–1680.

Möhler, O., A. Nink, H. Saathoff, S. Schaefers, M. Schnaiter, W. Schöck, and U. Schurath (2001), The Karlsruhe aerosol chamber facility AIDA: Technical discription and first results of homogeneous and heterogeneous ice nucleation experiments, in *Workshop on Ion-Aerosol-Cloud Interactions*, vol. 2001-007, edited by J. Kirkby, Eur. Organ. for Nucl. Res., Geneva.

Möhler, O., et al. (2003), Experimental investigation of homogeneous freezing of sulphuric acid particles in the aerosol chamber AIDA, *Atmos. Chem. Phys.*, *3*, 211–223.

Möhler, O., C. Linke, R. Wagner, A. Mangold, M. Krämer, H. Saathoff, M. Schnaiter, and U. Schurath (2005), Ice nucleation on flame soot aerosol of different organic carbon content, *Meteorol. Z.*, in press.

Nink, A., H. Saathoff, M. Schnaiter, and O. Möhler (2000), Laboratory investigation of the impact of aircraft particulate emissions on cirrus cloud formation, in *European Workshop on Aviation, Aerosols, Contrails, and Cirrus Clouds (A2C3)*, *Rep. 19428*, edited by U. Schumann and G. T. Amanatidis, pp. 149–153, EUR, Seeheim, Germany.

Paladino, J., P. Whitefield, D. Hagen, A. R. Hopkins, and M. Trueblood (1998), Particle concentration characterization for jet engine emissions under cruise conditions, *Geophys. Res. Lett.*, *25*(10), 1697–1700.

Penner, J. E., et al. (1999), *Aviation and the Global Atmosphere*, Cambridge Univ. Press, New York.

Petzold, A., and F. P. Schröder (1998), Jet engine exhaust aerosol characterization, *Aerosol Sci. Technol.*, *28*(1), 62–76.

Petzold, A., et al. (2003), Properties of jet engine combustion particles during the partemis experiment: Microphysics and chemistry, *Geophys. Res. Lett.*, *30*(13), 1719, doi:10.1029/2003GL017283.

Pruppacher, H. R., and J. D. Klett (1997), *Microphysics of Clouds and Precipitation*, Springer, New York.

Pueschel, R. F., S. Verma, G. V. Ferry, S. D. Howard, S. Vay, S. A. Kinne, J. Goodman, and A. W. Strawa (1998), Sulfuric acid and soot particle formation in aircraft exhaust, *Geophys. Res. Lett.*, *25*(10), 1685–1688.

Rahmes, T. F., A. H. Omar, and D. J. Wuebbles (1998), Atmospheric distributions of soot particles by current and future aircraft fleets and resulting radiative forcing on climate, *J. Geophys. Res.*, *103*(D24), 31,657–31,667.

Saathoff, H., O. Möhler, U. Schurath, S. Kamm, B. Dippel, and D. Mihelcic (2003), The AIDA soot aerosol characterisation campaign 1999, *J. Aerosol Sci.*, *34*(10), 1277–1296.

Sassen, K., and G. C. Dodd (1988), Homogeneous nucleation rate for highly supercooled cirrus cloud droplets, *J. Atmos. Sci.*, *45*(8), 1357–1369.

Sassen, K., M. K. Griffin, and G. C. Dodd (1989), Optical-scattering and microphysical properties of subvisual cirrus clouds, and climatic implications, *J. Appl. Meteorol.*, *28*(2), 91–98.

Schnaiter, M., H. Horvath, O. Möhler, K. H. Naumann, H. Saathoff, and O. W. Schöck (2003), Uv-vis-nir spectral optical properties of soot and soot-containing aerosols, *J. Aerosol Sci.*, *34*(10), 1421–1444.

Schröder, F. P., B. Kärcher, A. Petzold, R. Baumann, R. Busen, C. Hoell, and U. Schumann (1998), Ultrafine aerosol particles in aircraft plumes: In situ observations, *Geophys. Res. Lett.*, *25*(15), 2789–2792.

Schumann, U., et al. (2002), Influence of fuel sulfur on the composition of aircraft exhaust plumes: The experiments sulfur 1–7, *J. Geophys. Res.*, *107*(D15), 4247, doi:10.1029/2001JD000813.

Seifert, M., R. Tiede, M. Schnaiter, C. Linke, O. Möhler, U. Schurath, and J. Ström (2004), Operation and performance of a differential mobility particle sizer and a TSI 3010 condensation particle counter at stratospheric temperatures and pressures, *J. Aerosol Sci.*, *35*(8), 981–993.

Tabazadeh, A., O. B. Toon, and E. J. Jensen (1997), Formation and implications of ice particle nucleation in the stratosphere, *Geophys. Res. Lett.*, *24*(16), 2007–2010.

Twohy, C. H., and B. W. Gandrud (1998), Electron microscope analysis of residual particles from aircraft contrails, *Geophys. Res. Lett.*, *25*(9), 1359–1362.

Verein Deutscher Ingenieure (1999), Measurement of soot (ambient air): Thermographic determination of elemental carbon after thermal desorption of organic carbon, in *VDI/DIN-Handbuch Reinhaltung der Luft*, vol. 4, Beuth, Berlin.

Wagner, R., A. Mangold, O. Möhler, H. Saathoff, M. Schnaiter, and U. Schurath (2003), A quantitative test of infrared optical constants for supercooled sulphuric and nitric acid droplet aerosols, *Atmos. Chem. Phys.*, *3*, 1147–1164.

Zöger, M., et al. (1999), Fast in situ stratospheric hygrometers: A new family of balloon-borne and airborne Lyman α photofragment fluorescence hygrometers, *J. Geophys. Res.*, *104*(D1), 1807–1816.

Zuberi, B., A. K. Bertram, C. A. Cassa, L. T. Molina, and M. J. Molina (2002), Heterogeneous nucleation of ice in $(NH_4)_2SO_4$-H_2O particles

with mineral dust immersions, *Geophys. Res. Lett.*, *29*(10), 1504, doi:10.1029/2001GL014289.

S. Büttner, C. Linke, O. Möhler, H. Saathoff, M. Schnaiter, U. Schurath, O. Stetzer, and R. Wagner, Institute of Meteorology and Climate Research, Forschungszentrum Karlsruhe, Postfach 3640, D-76021 Karlsruhe, Germany. (ottmar.moehler@imk.fzk.de)

V. Ebert, Physikalisch-Chemisches Institut, Universität Heidelberg, Im Neuenheimer Feld 253, D-69120 Heidelberg, Germany.

M. Krämer and A. Mangold, Institut für Chemie und Dynamik der Geosphäre I, Forschungszentrum Jülich, D-52425 Jülich, Germany.